

Convergence of Calderón residuals

R. Hiptmair¹, C. Urzúa-Torres², A. Wisse²

¹Seminar for Applied Mathematics, ETH Zurich,
Rämistrasse 101, 8092 Zürich, Switzerland.

²Delft Institute of Applied Mathematics, TU Delft,
Mekelweg 4, 2628CD Delft, The Netherlands

Abstract

In this paper, we describe a framework to compute expected convergence rates for residuals based on the Calderón identities for general second order differential operators for which fundamental solutions are known. The idea is that these rates could be used to validate implementations of boundary integral operators and allow to test operators separately by choosing solutions where parts of the Calderón identities vanish. Our estimates rely on simple vector norms, and thus avoid the use of hard-to-compute norms and the residual computation can be easily implemented in existing boundary element codes. We test the proposed Calderón residuals as debugging tool by introducing artificial errors into the Galerkin matrices of some of the boundary integral operators for the Laplacian and time-harmonic Maxwell's equations. From this, we learn that our estimates are not sharp enough to always detect errors, but still provide a simple and useful debugging tool in many situations.

1 Introduction

Boundary integral equations (BIEs) and boundary element methods are popular when dealing with problems on unbounded domains and for which a fundamental solution is available. What is considerably less popular among practitioners and students is to validate and debug a boundary element code. On the one hand, the reality that one needs to handle singular integral adds complexity to the implementation (and thus additional places where things can go wrong). On the other hand, the fact that convergence rates for Galerkin discretizations of boundary integral equations are in fractional and even negative norms, make them an “all-or-nothing-tool” for code validation, and hence not truly useful for debugging. Indeed, if the Galerkin matrices are correctly implemented, one can typically choose a reference solution and use some of the matrices to measure the error via exploiting the norm equivalence between the solution space of the boundary integral equation and the energy norm of the operator. If the observed convergence rate agrees with the expected one, one knows that the implementation is correct. This, however, does not work if the implementation of the Galerkin matrix is incorrect, but how can we assess this in the first place?

In this paper, we describe a framework to compute expected convergence rates for residuals based on the Calderón identities for general second order differential operators for which fundamental solutions are known. The idea is that these rates could be used to validate implementations of boundary integral operators and allow to test operators separately by choosing solutions where parts of the Calderón identities vanish. Our estimates rely on simple vector norms, and thus avoid the use of hard-to-compute norms and the residual computation can be easily implemented in existing boundary element codes.

Outline

To illustrate the idea, we consider the general case first and, after this, fill in the details for the Laplace equation and time harmonic Maxwell's equations. We also provide several numerical experiments with correct and defective matrices to investigate the performance of the proposed *Calderón residuals* to detect implementation errors. It turns out that our estimates are not sharp enough to capture everything, but, given their implementation simplicity, we believe they are still worth trying in some cases.

2 General Case

Let $\Omega \subset \mathbb{R}^d$ for $d = 2, 3$ be a bounded domain with Lipschitz boundary $\Gamma = \partial\Omega$. We consider a second order partial differential equation of the type

$$\begin{cases} \mathcal{L}u = 0 & \text{in } \mathbb{R}^d \setminus \bar{\Omega}, \\ & \text{+ boundary conditions on } \Gamma, \\ & \text{+ radiation conditions at } \infty, \end{cases} \quad (2.1)$$

which we want to solve using boundary integral equations.

Let \mathbf{C} be the Calderón projector associated to the BIEs for \mathcal{L} and $\boldsymbol{\gamma}$ the Cauchy trace operator comprising of the Dirichlet-type trace γ_0 and the Neumann-type trace γ_1 . Then, the corresponding exterior Calderón identity is given by

$$\mathbf{C}\boldsymbol{\gamma} = \boldsymbol{\gamma} \iff (\mathbf{C} - \mathbf{Id})\boldsymbol{\gamma} = 0, \quad (2.2)$$

where \mathbf{Id} denotes the identity operator. For now, we want to express this in the most general way possible. Therefore, we write

$$\mathbf{C} := \begin{pmatrix} \mathbf{A}_1 + \frac{1}{2} \mathbf{Id} & \mathbf{A}_2 \\ \mathbf{A}_3 & \mathbf{A}_4 + \frac{1}{2} \mathbf{Id} \end{pmatrix}, \quad \boldsymbol{\gamma} = \begin{pmatrix} \gamma_0 u \\ \gamma_1 u \end{pmatrix},$$

where \mathbf{A}_i are the boundary integral operators (BIOS) related to \mathcal{L} and $\boldsymbol{\gamma}$. We have that

$$\begin{aligned} \mathbf{A}_1 : X_0 &\rightarrow X_0, & \mathbf{A}_2 : X_1 &\rightarrow X_0, \\ \mathbf{A}_3 : X_0 &\rightarrow X_1, & \mathbf{A}_4 : X_1 &\rightarrow X_1, \end{aligned}$$

where X_0 and X_1 are suitable Hilbert spaces on the boundary Γ such that X'_0 and X_1 are isomorphic, and $\mathbf{A}_1, \dots, \mathbf{A}_4$ are continuous operators and the traces γ_0 and γ_1 are also continuous.

If u is a solution to (2.1), then (2.2) implies

$$(\mathbf{A}_1 - \frac{1}{2} \mathbf{Id})\gamma_0 u + \mathbf{A}_2 \gamma_1 u = 0 \quad \text{in } X_0, \quad (2.3a)$$

$$\mathbf{A}_3 \gamma_0 u + (\mathbf{A}_4 - \frac{1}{2} \mathbf{Id})\gamma_1 u = 0 \quad \text{in } X_1 \quad (2.3b)$$

hold exactly. We can use (2.3) for code validation by testing

$$(\mathbf{A}_1 - \frac{1}{2} \mathbf{Id})\mathcal{I}_0 \gamma_0 u + \mathbf{A}_2 \mathcal{I}_1 \gamma_1 u \approx 0, \quad (2.4a)$$

$$\mathbf{A}_3 \mathcal{I}_0 \gamma_0 u + (\mathbf{A}_4 - \frac{1}{2} \mathbf{Id})\mathcal{I}_1 \gamma_1 u \approx 0, \quad (2.4b)$$

where \mathcal{I}_0 and \mathcal{I}_1 are operators that map the traces $\gamma_0 u$ and $\gamma_1 u$ to suitable finite dimensional subspaces. They can be interpolators or projections, but for simplicity we will refer to them as interpolants. Why “ \approx ” now? This is because in general the interpolants will not lie in the kernel of $(\mathbf{C} - \mathbf{Id})$. Yet we can expect them to be close, thus checking this can

provide evidence for the correctness of a BEM code. More precisely, failing to see “ ≈ 0 ” in (2.4) will indicate errors.

To grasp what this means in quantitative terms, let us consider a family of dyadically refined meshes $(\mathcal{G}_h)_{h \in \mathbb{H}}$ of Γ , where the index h denotes the corresponding meshwidth. Then, for each $h \in \mathbb{H}$, let

$$X_{0,h} \subset X_0, \quad X_{1,h} \subset X_1$$

define (conforming) boundary element spaces on the mesh \mathcal{G}_h such that the approximation of X_i by $X_{i,h}$ improves when $h \rightarrow 0$. Next, we introduce interpolation operators (‘boundary element interpolants’)

$$\mathcal{I}_0 : \mathcal{D}(X_0) \subset X_0 \rightarrow X_{0,h}, \quad \mathcal{I}_1 : \mathcal{D}(X_1) \subset X_1 \rightarrow X_{1,h}$$

mapping to the finite-dimensional subspaces. With this, we define the *Calderón residuals* as

$$r_0(\psi) := \int_{\Gamma} [(\mathbf{A}_1 - \frac{1}{2} \mathbf{Id}) \mathcal{I}_0 \gamma_0 u + \mathbf{A}_2 \mathcal{I}_1 \gamma_1 u] \psi \, d\Gamma, \quad \psi \in X_1, \quad (2.5a)$$

$$r_1(\phi) := \int_{\Gamma} [\mathbf{A}_3 \mathcal{I}_0 \gamma_0 u + (\mathbf{A}_4 - \frac{1}{2} \mathbf{Id}) \mathcal{I}_1 \gamma_1 u] \phi \, d\Gamma, \quad \phi \in X_0. \quad (2.5b)$$

By the approximation property of our finite-dimensional subspaces, we expect these residuals to become small when $h \rightarrow 0$. In order to quantify how this happens, it is easier to consider the rewritten forms

$$\begin{aligned} r_0(\psi) &= \int_{\Gamma} [(\mathbf{A}_1 - \frac{1}{2} \mathbf{Id})(\mathcal{I}_0 - \mathbf{Id}) \gamma_0 u + \mathbf{A}_2 (\mathcal{I}_1 - \mathbf{Id}) \gamma_1 u] \psi \, d\Gamma, \\ r_1(\phi) &= \int_{\Gamma} [\mathbf{A}_3 (\mathcal{I}_0 - \mathbf{Id}) \gamma_0 u + (\mathbf{A}_4 - \frac{1}{2} \mathbf{Id})(\mathcal{I}_1 - \mathbf{Id}) \gamma_1 u] \phi \, d\Gamma, \end{aligned}$$

which are obtained by subtracting the weak forms of (2.3a) and (2.3b) from (2.5a) and (2.5b), respectively, so that we can use existing results to compute a convergence rate. In other words, we bound the residuals by

$$\begin{aligned} |r_0(\psi)| &\leq [\|\mathbf{A}_1 - \frac{1}{2} \mathbf{Id}\|_{X_0 \rightarrow X_0} \|(\mathcal{I}_0 - \mathbf{Id}) \gamma_0 u\|_{X_0} \\ &\quad + \|\mathbf{A}_2\|_{X_1 \rightarrow X_0} \|(\mathcal{I}_1 - \mathbf{Id}) \gamma_1 u\|_{X_1}] \|\psi\|_{X'_0}, \\ |r_1(\phi)| &\leq [\|\mathbf{A}_3\|_{X_0 \rightarrow X_1} \|(\mathcal{I}_0 - \mathbf{Id}) \gamma_0 u\|_{X_0} \\ &\quad + \|\mathbf{A}_4 - \frac{1}{2} \mathbf{Id}\|_{X_1 \rightarrow X_1} \|(\mathcal{I}_1 - \mathbf{Id}) \gamma_1 u\|_{X_1}] \|\phi\|_{X'_1}. \end{aligned} \quad (2.6)$$

Since estimates of the type

$$\|(\mathcal{I}_i - \mathbf{Id})w\|_{X_i} \leq h^{\alpha_i} \|w\|_{\mathcal{X}_i}, \quad i = 0, 1,$$

with $\|\cdot\|_{\mathcal{X}_i}$ some appropriate norm, are usually available, then it only remains to estimate the test functions when these are taken in the finite-dimensional subspaces as mentioned above. For this, let $\{\beta_i, i = 1, \dots, N_0\}$ and $\{b_j, j = 1, \dots, N_1\}$ be bases of $X_{0,h}$ and $X_{1,h}$, respectively. With this, we define the *residual vectors*

$$\boldsymbol{\rho}_0 := [r_0(\beta_i)]_{i=1}^{N_0}, \quad (2.7)$$

$$\boldsymbol{\rho}_1 := [r_1(b_j)]_{j=1}^{N_1}. \quad (2.8)$$

Hence, we need to bound $\|\beta_i\|_{X_0}$ and $\|b_j\|_{X_1}$ and by combining this with (2.6) we know how the residual vectors will change with h . Consequently, one can use these convergence rates to deduce if the Galerkin matrices for the different BIOs are implemented

correctly by employing a manufactured solution to the exterior BVP (2.1); calculating the traces exactly, and finally letting the code compute the residuals and checking whether the observed rate agrees with the expected one.

Remark. *We can proceed analogously and use the interior Calderón identities instead of the exterior ones. Although for the sake of brevity we will not write the corresponding computations, it is worth mentioning that the estimates follow analogously and that this allows the practitioner to choose how to test their code depending on the analytical or manufactured solutions available. We will show examples regarding both interior and exterior Calderón identities when we do numerical experiments in later sections.*

3 First Application: Laplacian

Let us begin by looking for u such that $-\Delta u = 0$ in $\mathbb{R}^d \setminus \bar{\Omega}$ and the decay condition $u(\mathbf{x}) = \mathcal{O}(\|\mathbf{x}^{-1}\|)$ as $\|\mathbf{x}\| \rightarrow \infty$ is verified. This means that its weak solution $u \in H_{loc}^1(\Omega)$, and thus, that we consider the Dirichlet trace $\tau_D : H^1(\Omega) \rightarrow H^{1/2}(\Gamma)$, the Neumann trace $\tau_N : H_{loc}^1(\Omega) \rightarrow H^{-1/2}(\Gamma)$, and the related BIOs¹

- $\mathbf{V} : H^{-1/2}(\Gamma) \rightarrow H^{1/2}(\Gamma)$ (weakly singular);
- $\mathbf{W} : H^{1/2}(\Gamma) \rightarrow H^{-1/2}(\Gamma)$ (hypersingular);
- $\mathbf{K} : H^{1/2}(\Gamma) \rightarrow H^{1/2}(\Gamma)$ (double layer);
- $\mathbf{K}' : H^{-1/2}(\Gamma) \rightarrow H^{-1/2}(\Gamma)$ (adjoint double layer).

Hence, we have that, related to (2.1) and (2.2), $\mathcal{L} = -\Delta$, $\gamma_0 = \tau_D$ and $\gamma_1 = \tau_N$. In particular, the following identities are true for the Dirichlet and Neumann trace of u for the exterior BVP:

$$\begin{pmatrix} \frac{1}{2} \mathbf{Id} + \mathbf{K} & -\mathbf{V} \\ -\mathbf{W} & \frac{1}{2} \mathbf{Id} - \mathbf{K}' \end{pmatrix} \begin{pmatrix} \tau_D u \\ \tau_N u \end{pmatrix} = \begin{pmatrix} \tau_D u \\ \tau_N u \end{pmatrix} \iff \begin{pmatrix} \frac{1}{2} \mathbf{Id} - \mathbf{K} & \mathbf{V} \\ \mathbf{W} & \frac{1}{2} \mathbf{Id} + \mathbf{K}' \end{pmatrix} \begin{pmatrix} \tau_D u \\ \tau_N u \end{pmatrix} = 0. \quad (3.1)$$

Next, we proceed to discretize, which requires us to define our boundary element spaces.

Definition 3.1 ([8, Definitions 4.1.36, 4.1.17]). *Let Γ be a piecewise smooth surface and let \mathcal{G}_h be a regular surface mesh of Γ consisting of triangles. Let $\chi = \{\chi_\tau : \tau \in \mathcal{G}_h\}$ be a mapping vector and let $p \in \mathbb{N}_0$. We first introduce*

$$\mathbb{P}_p^\Delta := \text{span}\{\xi^\mu : \mu \in \mathbb{N}_0^2 \wedge |\mu| \leq p\}.$$

Then, we define for $p \in \mathbb{N}_0$

$$\mathcal{S}^{p,-1}(\mathcal{G}_h) := \{\psi : \Gamma \rightarrow \mathbb{K} : \forall \tau \in \mathcal{G}_h, \psi \circ \chi_\tau \in \mathbb{P}_p^\Delta\},$$

and for $p \geq 1$

$$\mathcal{S}^{p,0}(\mathcal{G}_h) := \{\psi \in C^0(\Gamma) : \forall \tau \in \mathcal{G}_h, \psi|_\tau \circ \chi_\tau \in \mathbb{P}_p^\Delta\}.$$

We remind the reader that we have interpolation operators mapping from subspaces of our trace spaces to these BE spaces. Indeed, we write $\mathcal{I}_h^{p,0}$ for the nodal interpolation operator mapping to $\mathcal{S}^{p,0}(\mathcal{G}_h)$, and $\mathcal{I}_h^{p-1,-1}$ for the local L^2 projector to $\mathcal{S}_\mathcal{G}^{p-1,-1}$ for $p \geq 1$. We always let \mathcal{G}_h be a shape regular, quasi uniform family of meshes.

¹We refer to [8, Chapter 2] for the definitions of these Sobolev spaces.

Following the derivation from (2.5a) and (2.5b), equation (3.1) leads to the following residuals

$$\begin{aligned} r_D(\psi) &:= \int_{\Gamma} \left[\left(\frac{1}{2} \mathbf{Id} - \mathbf{K} \right) \mathcal{I}_h^{p,0}(\tau_D u) + \mathbf{V}(\mathcal{I}_h^{p-1,-1} \tau_N u) \right] (x) \psi(x) dS(x) \\ &= \int_{\Gamma} \left[\left(\frac{1}{2} \mathbf{Id} - \mathbf{K} \right) (\mathcal{I}_h^{p,0} - \mathbf{Id})(\tau_D u) + \mathbf{V}((\mathcal{I}_h^{p-1,-1} - \mathbf{Id}) \tau_N u) \right] (x) \psi(x) dS(x), \end{aligned} \quad (3.2)$$

for $\psi \in H^{-1/2}(\Gamma)$, and

$$\begin{aligned} r_N(\phi) &:= \int_{\Gamma} \left[\mathbf{W} \mathcal{I}_h^{p,0}(\tau_D u) + \left(\frac{1}{2} \mathbf{Id} + \mathbf{K}' \right) \mathcal{I}_h^{p-1,-1} \tau_N u \right] (x) \phi(x) dS(x) \\ &= \int_{\Gamma} \left[\mathbf{W} (\mathcal{I}_h^{p,0} - \mathbf{Id})(\tau_D u) + \left(\frac{1}{2} \mathbf{Id} + \mathbf{K}' \right) (\mathcal{I}_h^{p-1,-1} - \mathbf{Id}) \tau_N u \right] (x) \phi(x) dS(x), \end{aligned} \quad (3.3)$$

for $\phi \in H^{1/2}(\Gamma)$.

Next step is to bound the residual as in (2.6). To do this we need the following results.

Assumption 3.2. *The following properties can hold for a surface Γ .*

1. Γ is the surface of a polyhedron. Its mesh \mathcal{G} consist of plane panels with straight edges with meshwidth $h > 0$.
2. Γ is a curved surface. Then we need certain geometric assumptions, see [8, Assumption 4.3.18].

Theorem 3.3 ([8, Theorem 4.3.20]). *Let Γ fulfill either of the conditions in Assumption 3.2. Then, we have for the interpolation $\mathcal{I}_h^{p-1,-1} : L^2(\Gamma) \rightarrow \mathcal{S}_{\mathcal{G}}^{p-1,-1}$ and $0 \leq t \leq s \leq p$ and all $u \in H_{pw}^s(\Gamma)$ (where this space is as defined in [8, Definition 4.1.48]) the estimate*

$$\|u - \mathcal{I}_h^{p-1,-1} u\|_{H^{-t}(\Gamma)} \leq Ch^{s+t} \|u\|_{H^s(\Gamma)}. \quad (3.4)$$

Theorem 3.4 ([8, Theorem 4.3.22b]). *Let Γ fulfill either of the conditions in Assumption 3.2. Let $u \in H^s(\Gamma)$ for some $1 < s \leq p+1$. Then, for any $0 \leq t \leq 1$, we have*

$$\|u - \mathcal{I}_h^{p,0} u\|_{H^t(\Gamma)} \leq Ch^{s-t} \|u\|_{H^s(\Gamma)}. \quad (3.5)$$

Theorem 3.5. *Let $q_N^j, j = 1, \dots, N_0$, be a set of nodal basis functions of $\mathcal{S}^{p-1,-1}(\mathcal{G}_h)$, and let $\varphi_N^i, i = 1, \dots, N_1$, be a set of nodal basis functions of $\mathcal{S}^{p,0}(\mathcal{G}_h)$. Let r_D and r_N be as introduced in (3.2) and (3.3), and define*

$$\boldsymbol{\rho}_D := [r_D(q_N^j)]_{j=1}^{N_0}, \quad \boldsymbol{\rho}_N := [r_N(\varphi_N^i)]_{i=1}^{N_1}.$$

Then, it holds that

$$\boxed{\begin{aligned} \|\boldsymbol{\rho}_D\|_{\infty} &= \mathcal{O}(h^{p+\frac{1}{2}+\frac{d}{2}}), & \|\boldsymbol{\rho}_N\|_{\infty} &= \mathcal{O}(h^{p-\frac{1}{2}+\frac{d}{2}}), \\ \|\boldsymbol{\rho}_D\|_2 &= \mathcal{O}(h^{p-\frac{1}{2}+\frac{d}{2}}), & \|\boldsymbol{\rho}_N\|_2 &= \mathcal{O}(h^{p-\frac{3}{2}+\frac{d}{2}}). \end{aligned}}$$

Proof. From Equations (3.2), (3.3), we get

$$\begin{aligned} |r_D| &\leq \left[\left\| \frac{1}{2} \mathbf{Id} + \mathbf{K} \right\|_{H^{1/2}(\Gamma) \rightarrow H^{1/2}(\Gamma)} \|(\mathcal{I}_h^{p,0} - \mathbf{Id}) \tau_D u\|_{H^{1/2}(\Gamma)} \right. \\ &\quad \left. + \|\mathbf{V}\|_{H^{-1/2}(\Gamma) \rightarrow H^{1/2}(\Gamma)} \|(\mathcal{I}_h^{p-1,-1} - \mathbf{Id}) \tau_N u\|_{H^{-1/2}(\Gamma)} \right] \|\psi\|_{H^{-1/2}(\Gamma)}, \\ |r_N| &\leq \left[\left\| \mathbf{W} \right\|_{H^{1/2}(\Gamma) \rightarrow H^{-1/2}(\Gamma)} \|(\mathcal{I}_h^{p,0} - \mathbf{Id}) \tau_D u\|_{H^{1/2}(\Gamma)} \right. \\ &\quad \left. + \left\| \frac{1}{2} \mathbf{Id} + \mathbf{K}' \right\|_{H^{-1/2}(\Gamma) \rightarrow H^{-1/2}(\Gamma)} \|(\mathcal{I}_h^{p-1,-1} - \mathbf{Id}) \tau_N u\|_{H^{-1/2}(\Gamma)} \right] \|\phi\|_{H^{1/2}(\Gamma)}. \end{aligned}$$

Using the continuity of the BIOs and Theorems 4.3.20 and 4.3.22b from [8], this can be rewritten as

$$|r_D| \leq c_D h^{p+\frac{1}{2}} \|\psi\|_{H^{-1/2}(\Gamma)}, \quad |r_N| \leq c_R h^{p+\frac{1}{2}} \|\phi\|_{H^{1/2}(\Gamma)} \quad (3.6)$$

for some h -independent constants $c_D, c_R > 0$.

Now we replace ψ with q_N^j and ϕ with φ_N^i . We illustrate the procedure for $d = 3$. Firstly, let $\pi \in \mathcal{G}_h$ be a panel of diameter h . Then, for the reference triangle \hat{K} , we have some fixed reference shape function \hat{q}^j , which is the pullback of the basis function q_N^j to \hat{K} , such that

$$\begin{aligned} \|q_N^j\|_{H^{-1/2}(\Gamma)}^2 &\simeq \int_{\Gamma} \nabla(q_N^j)(x) q_N^j(x) dS(x) = \int_{\pi} \int_{\pi} \frac{1}{4\pi\|x-y\|} q_N^j(y) q_N^j(x) dS(x) dS(y) \\ &= h^{2\cdot 2} \int_{\hat{K}} \int_{\hat{K}} \frac{1}{4\pi h\|s-t\|} \hat{q}^j(s) \hat{q}^j(t) dt ds = \mathcal{O}(h^3), \end{aligned}$$

where \simeq denotes equality up to a constant, which in this case follows from ∇ being continuous and elliptic in $H^{-1/2}(\Gamma)$. Similar arguments work for $d = 2$. Hence, we have that

$$\|q_N^j\|_{H^{-1/2}(\Gamma)} \approx h^{\frac{d}{2}} \quad \text{on } \mathcal{G}_h,$$

with constants independent of h . Secondly, we have that

$$\begin{aligned} \|\varphi_N^i\|_{H^{1/2}(\Gamma)}^2 &\simeq \int_{\Gamma} (\nabla \varphi_N^i)(x) \varphi_N^i(x) dS(x) \\ &= \int_{\pi} \int_{\pi} \frac{1}{4\pi\|x-y\|} \mathbf{curl}_{\Gamma} \varphi_N^i(y) \cdot \mathbf{curl}_{\Gamma} \varphi_N^i(x) dS(x) dS(y). \end{aligned}$$

Thus, using that the curl scales like h under scaling pullback to the reference triangle \hat{K} , the same arguments as before yield

$$\|\varphi_N^i\|_{H^{1/2}(\Gamma)} \approx h^{\frac{d}{2}-1} \quad \text{on } \mathcal{G}_h.$$

Combining this with (3.6) gives the result. \square

3.1 Implementation and sanity checks

We calculate the residuals for some Examples using the library `Bempp`². We use the following solutions to $-\Delta u = 0$ on some domain Ω :

- **Example 1a:** Let Ω be the unit ball in \mathbb{R}^3 , then we consider the exact solution on $\mathbb{R}^3 \setminus \bar{\Omega}$ (in spherical coordinates)

$$u(r, \theta, \phi) = r^{-2} e^{i\phi} P_1^1(\cos \theta),$$

where $P_1^1(x) = -(1-x^2)^{1/2} \frac{d}{dx}(P_1(x))$, and $P_1(x)$ is the first degree Legendre polynomial. Then the Dirichlet and Neumann traces are, respectively, given by

$$\begin{aligned} \tau_D u(r, \theta, \phi) &= r^{-2} e^{i\phi} P_1^1(\cos \theta)|_{\Gamma} \\ \tau_N u(r, \theta, \phi) &= \frac{\partial}{\partial r} u(r, \theta, \phi)|_{\Gamma} = -2r^{-3} e^{i\phi} P_1^1(\cos \theta)|_{\Gamma}. \end{aligned}$$

²<https://bempp.com/>

- **Example 1b:** Let Ω be the unit ball in \mathbb{R}^3 , then we consider the exact solution (in spherical coordinates)

$$u(r, \theta, \phi) = r e^{i\phi} P_1^1(\cos \theta),$$

with $P_1^1(x)$ as before. Then the Dirichlet and Neumann traces are, respectively, given by

$$\begin{aligned}\tau_D u(r, \theta, \phi) &= r e^{i\phi} P_1^1(\cos \theta)|_{\Gamma} \\ \tau_N u(r, \theta, \phi) &= \frac{\partial}{\partial r} u(r, \theta, \phi)|_{\Gamma} = e^{i\phi} P_1^1(\cos \theta).\end{aligned}$$

- **Example 2:** Let Ω be the unit cube in \mathbb{R}^3 . We assume the exact solution is given by

$$u(x, y, z) = x^2 - \frac{1}{2}y^2 - \frac{1}{2}z^2.$$

Then the Dirichlet and Neumann trace are given by

$$\tau_D u = u|_{\Gamma}, \quad \tau_N u = \nabla u|_{\Gamma} \cdot \mathbf{n} = \begin{pmatrix} 2x \\ -y \\ -z \end{pmatrix} |_{\Gamma} \cdot \mathbf{n}.$$

Here, \mathbf{n} is the outward pointing normal vector.

Our motivation to consider these three examples as “canonical examples” is that they will give us information about the performance of the Calderón residuals for exterior problems (Example 1a) vs. interior problems (Examples 1b and 2); and extra regular solutions on a sphere (Examples 1a and 1b) vs. standard solution on a square (Example 2).

For our implementation, we use the lowest order spaces for all of the approximations, i.e., $\mathcal{S}^{1,0}(\mathcal{G}_h) \subset H^{1/2}(\Gamma)$ (piecewise linear functions) and $\mathcal{S}^{0,-1}(\mathcal{G}_h) \subset H^{-1/2}(\Gamma)$ (piecewise constant functions) for some mesh \mathcal{G}_h . We construct the Galerkin matrices for our boundary integral operators as usual.

3.1.1 Empiric convergence of norms of basis functions

# elements	$\max(\text{diag}(\mathbf{V}_h))$	$\max(\text{diag}(\mathbf{W}_h))$
128	1.261e-02	2.488e-01
512	1.797e-03	1.460e-01
2048	2.325e-04	7.70e-02
8192	2.932e-05	3.904e-02
observed conv. rate	3.00	0.92
expected conv. rate	3	1

Table 1: Maximal element on diagonal of \mathbf{V}_h and \mathbf{W}_h to numerically compute the norm of piecewise constant and piecewise linear basis functions.

First, we validate the predicted convergence rates of scalar basis functions. In particular, we compute the $H^{-1/2}(\Gamma)$ -norm for piecewise constants q_N^j , and the $H^{1/2}(\Gamma)$ -norm for piecewise linears φ_N^i . Since the weakly singular \mathbf{V} and hypersingular boundary integral operator \mathbf{W} induce energy norms on $H^{-1/2}(\Gamma)$ and $H^{\frac{1}{2}}(\Gamma)$, respectively, we calculate $\|q_N^j\|_{H^{-1/2}(\Gamma)}$ and $\|\varphi_N^i\|_{H^{1/2}(\Gamma)}$ by inspecting the diagonals of their Galerkin matrices \mathbf{V}_h

and \mathbf{W}_h . Note that this approach gives a measure of the square of the norms of the basis functions, and thus we compare them with two times the computed convergence estimate. The results are reported in Table 1. There, we see that the observed convergence rates for all of the basis functions are close to the expected ones. Here, the observed convergence rates are labelled 'observed conv. rate' and were computed using polyfit and taking the logarithm of the values reported in the columns.

3.1.2 Checking convergence of Calderón residuals

Tables 2, 3 and 4 show the obtained results with Bempp for Examples 1a, 1b and 2, respectively. In all Examples, the observed convergence is larger than expected, but this, of course, does not contradict the theory. Moreover, in light of the rates from Table 1, we have reason to believe this arises from the inequalities used to derive the estimate being too crude, and not from a mistake in the computed rates. We point out, however, that although our estimates are correct, this lack of sharpness may hamper the effectiveness of Calderón residuals as debugging tool, which is what we will study in the next section.

# elements	$\ \rho_D\ _\infty$	$\ \rho_D\ _2$	$\ \rho_N\ _\infty$	$\ \rho_N\ _2$
128	1.0025e-03	7.6619e-03	7.2558e-03	3.3546e-02
512	8.0813e-05	1.1109e-03	6.5674e-04	6.1615e-03
2048	5.9248e-06	1.5188e-04	4.2410e-05	8.3545e-04
8192	3.8476e-06	1.9611e-05	2.6599e-06	1.0904e-04
observed conv. rate	3.89	2.95	3.92	2.84
expected conv. rate	3	2	2	1

Table 2: Calderón residuals for Laplace BVP, considering Example 1a on the unit sphere.

# elements	$\ \rho_D\ _\infty$	$\ \rho_D\ _2$	$\ \rho_N\ _\infty$	$\ \rho_N\ _2$
128	5.4551e-04	3.7834e-03	2.6058e-03	1.3876e-02
512	4.1249e-05	5.3052e-04	2.1362e-04	2.2848e-03
2048	2.6771e-06	6.8635e-05	1.5945e-05	3.1756e-04
8192	1.7098e-07	8.6937e-06	1.6783e-06	4.2566e-05
observed conv. rate	3.99	3.004	3.65	2.87
expected conv. rate	3	2	2	1

Table 3: Calderón residuals for Laplace BVP, considering Example 1b on the unit sphere.

# elements	$\ \rho_D\ _\infty$	$\ \rho_D\ _2$	$\ \rho_N\ _\infty$	$\ \rho_N\ _2$
84	7.2364e-04	2.8750e-03	8.7829e-04	2.5842e-03
336	3.9060e-05	2.4859e-04	2.3016e-04	9.9100e-04
1344	2.7451e-05	2.3896e-05	2.0798e-05	1.6799e-04
5376	1.8921e-06	2.2553e-06	2.4550e-06	2.9649e-05
observed conv. rate	3.95	3.43	2.89	2.19
expected conv. rate	3	2	2	1

Table 4: Calderón residuals for Laplace BVP, considering Example 2 on the unit cube.

3.2 Numerical results when introducing artificial errors

We test how robust our method is by introducing artificial errors in the Galerkin matrices of the weakly singular \mathbf{V} and hypersingular boundary integral operator \mathbf{W} . We skip the double layer operators for brevity.

For each test, we calculate the Calderón residuals, compare them with the standard *method of manufactured solutions (MMS)* convergence test. In other words, we do the following convergence test: (i) We build the *correct* Galerkin matrices and store them as \mathbf{V}_h , \mathbf{K}_h and \mathbf{W}_h^m , where \mathbf{W}_h^m is the Galerkin matrix corresponding to the modified hypersingular boundary integral operator from [10, Equation 7.26] with $\bar{\alpha} = 1$. We also build the mass matrix \mathbf{M}_h arising from Id ; (ii) we introduce an artificial error in the computation of the matrices of \mathbf{V} or \mathbf{W} , and store these *defective* Galerkin matrices as \mathbf{V}_h^e and $\mathbf{W}_h^{m,e}$; (iii) We use CG with relative tolerance equal to 10^{-10} (or a direct solver when CG fails to converge³) to numerically solve the following linear systems

$$\mathbf{V}_h^e \vec{w} = \left(\frac{1}{2} \mathbf{M}_h + \mathbf{K}_h \right) (\mathcal{I}_h^{1,0} \tau_D u), \quad (3.7)$$

$$\mathbf{W}_h^{m,e} \vec{v} = \left(\frac{1}{2} \mathbf{M}_h - \mathbf{K}'_h \right) (\mathcal{I}_h^{0,-1} \tau_N u), \quad (3.8)$$

for the coefficient vectors \vec{w} and \vec{v} ; (iv) We measure the *MMS errors*

$$\mathbf{e}_N := \|\tau_N u - w_h\|_{H^{-1/2}(\Gamma)} \approx \|(\mathcal{I}_h^{0,-1} \tau_N u - \vec{w})^\top \mathbf{V}_h (\mathcal{I}_h^{0,-1} \tau_N u - \vec{w})\|^{1/2}, \quad (3.9)$$

$$\mathbf{e}_D := \|\tau_D u - v_h\|_{H^{1/2}(\Gamma)} \approx \|(\mathcal{I}_h^{1,0} \tau_D u - \vec{v})^\top \widetilde{\mathbf{W}}_h (\mathcal{I}_h^{1,0} \tau_D u - \vec{v})\|^{1/2}, \quad (3.10)$$

where w_h is the boundary element function with coefficients \vec{w} and v_h is the one corresponding to the coefficients \vec{v} , i.e. $w_h = \sum_i w_i \beta_i$ and $v_h = \sum_i v_i b_i$; and $\widetilde{\mathbf{W}}_h$ is the Galerkin matrix of the hypersingular integral operator for the Helmholtz operator with imaginary wavenumber; (v) Finally, we repeat steps (i)-(iv) for a sequence of dyadically refined meshes and see if this behaves like $h^{1/2}$ for (3.9) and like $h^{3/2}$ for (3.10), where h is the meshwidth as before.

We make this comparison to contextualize the performance of the Calderón residuals and assess if the information we get is meaningful. Since the Galerkin matrices for Example 1a and 1b are the same, and Tables 2 and 3 confirm that Calderón residuals behave qualitatively the same for an exterior BVP and its interior counterpart, we only test Examples 1a and 2 in this subsection. We report the convergence rate computed with linear regression and taking the logarithm of the values reported in the columns. This is reported for all quantities in the additional row ‘ooc’. The last row, labelled ‘eoc’ corresponds to the expected convergence rate and is provided to make the comparison easier. Given that sometimes \mathbf{e}_N and \mathbf{e}_D do not decay monotonically as expected, all tables where these errors are measured include the columns labelled ‘ooc \mathbf{e}_i ’, $i = D, N$, which contain the observed convergence rate calculated using the error of two consecutive meshsizes. In this way, the unexpected behaviours become evident. In the situations where the rate computed with linear regression and the one calculated between two consecutive meshes disagree, we consider the latter to be more relevant.

3.2.1 Inaccurate quadrature

We adapt the quadrature for Example 1a and Example 2. Standard parameters in **Bempp** are order 4 for both the singular and the regular quadrature. These are adapted to 1 for the

³Using a direct solver is in our case only necessary when the introduced artificial error breaks some fundamental ‘nice’ property of the system matrix, like positive definiteness.

singular and 2 for the regular quadrature, respectively. Table 5 shows that for the exterior extra regular problem (Example 1a), the *MMS* test from (3.9)-(3.10) gives values in the range of machine precision, while the *Calderón residual* test obtains observed convergence rates that are still close to or even higher than the expected ones. For the interior problem (Example 2), we see in Table 6 that the situation is a bit more complicated. For the *MMS* test we have that \mathbf{e}_N converges with the expected rate and \mathbf{e}_D does not. In this case, the *Calderón residual* test fails for both ρ_D and ρ_N . It is therefore not clear if we can use Calderón residuals to identify if the quadrature is precise enough.

N	$\ \rho_D\ _\infty$	$\ \rho_D\ _2$	$\ \rho_N\ _\infty$	$\ \rho_N\ _2$	\mathbf{e}_N , tol=10 ⁻¹⁰	ooc \mathbf{e}_N	\mathbf{e}_D , tol=10 ⁻¹⁰	ooc \mathbf{e}_D
128	2.090e-02	1.518e-01	1.571e-02	8.548e-02	4.784e-08		1.322e-07	
512	3.153e-03	4.038e-02	2.967e-03	2.587e-02	4.265e-08	0.58*	9.098e-08	2.83*
2048	4.322e-04	1.027e-02	4.650e-04	7.388e-03	2.699e-08	0.48*	6.546e-08	-2.95*
8192	5.480e-05	2.576e-03	6.426e-05	1.968e-03	4.235e-08	-1.28*	1.587e-07	2.02*
ooc	2.94	2.02	2.72	1.86	0.12*		-0.03*	
eoc	3	2	2	1	0.5	0.5	1.5	1.5

Table 5: Convergence results with **Bempp** for Laplace BVP, considering Example 1a on the unit sphere and using a less accurate quadrature.

*: Note that the values of \mathbf{e}_N and \mathbf{e}_D are in range of machine precision, hence the observed rate may be meaningless.

N	$\ \rho_D\ _\infty$	$\ \rho_D\ _2$	$\ \rho_N\ _\infty$	$\ \rho_N\ _2$	\mathbf{e}_N , tol=10 ⁻¹⁰	ooc \mathbf{e}_N	\mathbf{e}_D , tol=10 ⁻¹⁰	ooc \mathbf{e}_D
84	3.833e-02	1.572e-01	2.134e-01	6.977e-01	3.231e-01		3.544e-01	
336	1.341e-02	8.898e-02	6.814e-02	3.937e-01	2.166e-01	0.58	2.211e-01	0.68
1344	3.671e-03	4.733e-02	1.995e-02	2.084e-01	1.290e-01	0.75	1.247e-01	0.83
5376	9.534e-04	2.439e-02	5.688e-03	1.072e-01	7.199e-02	0.84	6.728e-02	0.90
ooc	1.79	0.90	1.75	0.90	0.72		0.80	
eoc	3	2	2	1	0.5	0.5	1.5	1.5

Table 6: Convergence results with **Bempp** for Laplace BVP, considering Example 2 on the unit cube and using a less accurate quadrature.

3.2.2 Perturbing entries in \mathbf{V}_h

We investigate what happens when we introduce the following artificial errors:

- [Error A] replacing the diagonal of \mathbf{V}_h with random numbers between 0 and 10,
- [Error B] scaling the diagonal of \mathbf{V}_h with a factor $\frac{1}{2}$,
- [Error C] scaling the diagonal of \mathbf{V}_h with a factor 10^3 ,
- [Error D] scaling the first half of the diagonal of \mathbf{V}_h with a factor 10^3 ,
- [Error E] scaling the diagonal of \mathbf{V}_h with a factor h^{-1} , where h is the meshwidth.

In this section, the residual norms for ρ_N are not calculated, since they are not affected when only adapting \mathbf{V}_h .

Error A: Table 7 reports the residuals ρ_D in infinity and Euclidean norm when *replacing the diagonal of \mathbf{V}_h with random numbers*. They also contain the corresponding errors from the MMS test, as described in (3.9). We see that, in both tables, the Calderón residuals have convergence rates that are much lower than the predicted rates. But the MMS test for Example 1a tells us that we do have convergence. The MMS test for Example 2 agrees with the convergence of the residuals. Note that this is only one instance of replacing the

diagonal of \mathbf{V}_h with random numbers.

Example 1a (unit sphere)				
# elements	$\ \rho_D\ _\infty$	$\ \rho_D\ _2$	e_N , tol= 10^{-10}	ooc e_N
128	2.0714e00	1.1570e01	8.3901e-01	
512	2.0233e00	2.2174e01	3.0698e-01	1.45
2048	1.9910e00	4.2904e01	2.3534e-01	0.38
8192	1.9948e00	8.5089e01	4.4270e-02	2.41
ooc	0.02	-0.99	1.3	
eoc	3	2	0.5	0.5

Example 2 (unit cube)				
# elements	$\ \rho_D\ _\infty$	$\ \rho_D\ _2$	e_N , tol= 10^{-10}	ooc e_N
84	1.9899e00	5.3918e00	8.0563e-01	
336	1.9840e00	1.0520e01	8.6620e-01	-0.10
1344	1.9899e00	2.1601e01	8.7636e-01	-0.02
5376	1.9991e00	4.2109e01	8.7828e-01	-0.003
ooc	-0.002	-0.99	-0.04	
eoc	3	2	0.5	0.5

Table 7: Convergence results with `Bempp` for one instance of the Laplace BVP and introducing **Error A** (replacing diagonal entries of \mathbf{V}_h with random numbers).

Example 1a (unit sphere)				
# elements	$\ \rho_D\ _\infty$	$\ \rho_D\ _2$	e_N , direct	ooc e_N
128	1.1163e-02	7.8460e-02	5.0246e-07	
512	1.5458e-03	1.9421e-02	1.9938e-07	1.33
2048	2.0229e-04	4.7858e-03	1.1956e-07	0.74
8192	2.5254e-05	1.1857e-03	1.6658e-07	-0.48
ooc	3.01	2.07	0.55	
eoc	3	2	0.5	0.5

Example 2 (unit cube)				
# elements	$\ \rho_D\ _\infty$	$\ \rho_D\ _2$	e_N , direct	ooc e_N
84	4.1716e-02	1.7853e-01	4.3362e00	
336	1.3861e-02	9.5410e-02	3.0417e00	0.51
1344	3.7277e-03	4.9033e-2	1.9252e00	0.66
5376	9.6080e-04	2.4821e-02	2.2635e00	-0.23
ooc	1.82	0.95	0.35	
eoc	3	2	0.5	0.5

Table 8: Convergence results with `Bempp` for Laplace BVP and introducing **Error B** (scaling diagonal of \mathbf{V}_h with factor $\frac{1}{2}$). Here, the *MMS* test is ran with a direct solver.

Error B: Table 8 shows the results when scaling the diagonal of \mathbf{V}_h with a factor $\frac{1}{2}$. In this case, CG does not converge, because the introduced error breaks the positive definiteness of the matrix. We refer the reader to Appendix C for further details. In order to still test what happens when the nice properties of the matrix are broken, we resorted to

using a direct solver instead. This substantial change in the matrix might also influence that the Calderón residuals pass the test, but the MMS test from (3.9) gives inconsistent results. From this example, we conclude that before implementing any of the two studied convergence tests, the practitioner should indeed check that the obtained matrix is symmetric positive definite, as we know it should be from the theory.

Error C: Table 9 displays the results when scaling the diagonal of \mathbf{V}_h with a factor 10^3 . At first glance, there seems to be an inconsistency between the Calderón residual test and the MMS test for Example 1a. However, the values of \mathbf{e}_N are in the range of machine precision. Hence, calculating a rate here may not make sense. Indeed, if we consider that having all errors within machine precision already means convergence, then both tests agree. For Example 2, we see that again the Calderón residuals do not detect the error, but this time, the MMS really does. One reason why this may be the case, is that the Calderón residual tests will fail to see errors whose influence decays faster than the convergence rate. This is the motivation behind **Error E** later, which seeks to test this hypothesis.

Example 1a (unit sphere)				
# elements	$\ \rho_D\ _\infty$	$\ \rho_D\ _2$	\mathbf{e}_N , tol= 10^{-10}	ooc \mathbf{e}_N
128	2.3134e01	1.4726e02	2.0481e-08	
512	3.0233e00	3.7342e01	2.9949e-08	-0.55*
2048	3.9756e-01	9.3715e00	3.0299e-08	-0.02*
8192	4.9968e-02	2.3452e00	4.2499e-08	-0.50*
ooc	3.03	2.05	-0.33*	
eoc	3	2	0.5	0.5

Example 2 (unit cube)				
# elements	$\ \rho_D\ _\infty$	$\ \rho_D\ _2$	\mathbf{e}_N , tol= 10^{-10}	ooc \mathbf{e}_N
84	1.3152e01	4.2215e01	8.7817e-01	
336	1.6526e00	1.0596e01	8.7556e-01	0.004
1344	2.0858e-01	2.6702e00	8.7045e-01	0.01
5376	2.6567e-02	6.7815e-01	8.6049e-01	0.02
ooc	2.98	1.97	0.01	
eoc	3	2	0.5	0.5

Table 9: Convergence results with **Bempp** for Laplace BVP and introducing **Error C** (scaling diagonal of \mathbf{V}_h with factor 10^3).

*: Note that the values of \mathbf{e}_N for Example 1a are in range of machine precision, hence the observed rate may be meaningless.

Error D: Table 10 summarizes the results when scaling the first half of the diagonal of \mathbf{V}_h with a factor 10^3 . We see in both examples that the convergence rate of Calderón residuals is approximately equal to the expected one, and that the MMS test tells us that we do not have convergence. The observed behaviour is similar to what we obtained for **Error C**. We will check in the next experiment if we can improve the agreement between the two tests by introducing an error that is h -dependent.

Example 1a (unit sphere)				
# elements	$\ \rho_D\ _\infty$	$\ \rho_D\ _2$	e_N , tol= 10^{-10}	ooc e_N
128	2.3135e01	1.0413e02	9.8562e-09	
512	3.0233e00	2.6404e01	5.9872e-08	-2.60*
2048	3.9756e-01	6.2667e00	4.7220e-08	0.34*
8192	4.9968e-02	1.6583e00	4.2289e-08	0.16*
ooc	2.95	2.0	-0.6*	
eoc	3	2	0.5	0.5

Example 2 (unit cube)				
# elements	$\ \rho_D\ _\infty$	$\ \rho_D\ _2$	e_N , tol= 10^{-10}	ooc e_N
84	1.3104e01	3.4270e01	7.5909e-01	
336	1.6380e00	8.5672e00	7.4645e-01	0.02
1344	2.0475e-01	2.1418e00	7.3703e-01	0.02
5376	2.5593e-02	5.3545e-01	7.2576e-01	0.02
ooc	3.00	2.00	0.02	
eoc	3	2	0.5	0.5

Table 10: Convergence results with **Bempp** for Laplace BVP and introducing **Error D** (scaling first half of the diagonal of \mathbf{V}_h with factor 10^3).

*: Note that the values of e_N for Example 1a are in range of machine precision, hence the observed rate may be meaningless.

Example 1a (unit sphere)				
# elements	$\ \rho_D\ _\infty$	$\ \rho_D\ _2$	e_N , tol= 10^{-10}	ooc e_N
128	2.9101e-02	1.7769e-01	2.0110e-08	
512	1.2081e-02	1.4881e-01	4.2862e-08	-1.09*
2048	3.8291e-03	9.0247e-02	4.3826e-08	-0.03*
8192	1.0467e-03	4.9126e-02	6.0315e-08	-0.46*
ooc	1.65	0.65	-0.49*	
eoc	3	2	0.5	0.5

Example 2 (unit cube)				
# elements	$\ \rho_D\ _\infty$	$\ \rho_D\ _2$	e_N , tol= 10^{-10}	ooc e_N
84	6.6493e-02	2.4767e-01	3.4313e-01	
336	2.0875e-02	1.3496e-01	3.8876e-01	-0.18
1344	5.5837e-03	7.0075e-02	4.0989e-01	-0.008
5376	1.4376e-03	3.5667e-02	4.2018e-01	-0.04
ooc	1.85	0.93	-0.10	
eoc	3	2	0.5	0.5

Table 11: Convergence results with **Bempp** for Laplace BVP and introducing **Error E** (scaling diagonal of \mathbf{V}_h with factor h^{-1}).

*: Note that the values of e_N for Example 1a are in range of machine precision, hence the observed rate may be meaningless.

Error E: Table 11 shows the results when scaling the diagonal of \mathbf{V} with a factor h^{-1} . We see that in both Examples the convergence rate of the Calderón residuals is below the expected one, and that the energy norm test tells us that we do not expect convergence.

But, as we have seen before, the values of \mathbf{e}_N for Example 1a are again in the range of machine precision, which means that we have convergence. Hence, for Example 2, the two tests agree and are able to detect that there is a problem, but for Example 1a the tests disagree.

3.2.3 Perturbing entries in \mathbf{W}_h

We investigate what happens when we introduce the same artificial errors as before but now for the hypersingular operator \mathbf{W} , i.e.:

- [Error A] replacing the diagonal of \mathbf{W}_h with random numbers between 0 and 10,
- [Error B] scaling the diagonal of \mathbf{W}_h with a factor $\frac{1}{2}$,
- [Error C] scaling the diagonal of \mathbf{W}_h with a factor 10^3 ,
- [Error D] scaling the first half of the diagonal of \mathbf{W}_h with a factor 10^3 ,
- [Error E] scaling the diagonal of \mathbf{W}_h with a factor h^{-1} , where h is the meshwidth.

In this section, the residual norms for ρ_D are not calculated, since they are not affected when adapting \mathbf{W}_h .

Example 1a (unit sphere)				
# elements	$\ \rho_N\ _\infty$	$\ \rho_N\ _2$	\mathbf{e}_D , tol= 10^{-10}	ooc \mathbf{e}_D
128	7.5889e-01	2.8135e00	3.4701e01	
512	8.9943e-01	6.3053e00	1.1577e01	1.58
2048	9.5124e-01	1.3971e01	1.7186e03	-7.21
8192	9.7547e-01	2.854e01	6.2075e00	8.11
ooc	-0.12	-1.15	0.04	
eoc	2	1	1.5	1.5

Example 2 (unit cube)				
# elements	$\ \rho_N\ _\infty$	$\ \rho_N\ _2$	\mathbf{e}_D , tol= 10^{-10}	ooc \mathbf{e}_D
84	6.8970e-01	1.2594e00	2.2994e00	
336	8.6444e-01	3.1304e00	7.9503e00	-1.79
1344	8.9094e-01	6.6847e00	7.4968e00	0.08
5376	9.2668e-01	1.3733e01	1.3001e01	-0.79
ooc	-0.13	-1.1	-0.7	
eoc	2	1	1.5	1.5

Table 12: Convergence results with `Bempp` for Laplace BVP and introducing **Error A** (replacing diagonal of \mathbf{W}_h with random numbers).

In Tables 12-16 we see that the observed convergence rates for Calderón residuals are lower than the expected ones, which means the Calderón residual test detects all the introduced errors that we tried. We see in Tables 12 and 13 that the convergence rates for \mathbf{e}_D in Example 1a are fluctuating. This might be because in Table 12, the introduced error is done with random numbers, and it could happen that we get a 'worse' matrix for some realizations of this. In Table 13 we have the same problem as when we are introducing **Error B** for \mathbf{V}_h in Table 8, where scaling the diagonal of the matrix destroys the good properties of the matrix. Furthermore, in Tables 14 and 16 for Example 1a, we see that \mathbf{e}_D has values in the range of machine precision, so that calculating a convergence rate

does not give us much information. In all other cases, the convergence rate of e_D is lower than expected, thus matching the predictions from the residuals.

Example 1a (unit sphere)				
# elements	$\ \rho_N\ _\infty$	$\ \rho_N\ _2$	e_D , tol= 10^{-10}	ooc e_D
128	1.3139e-01	8.1555e-01	1.6947e-06	
512	6.7798e-02	8.0597e-01	1.3986e-07	3.84
2048	3.4590e-02	8.0308e-01	6.4068e-07	-2.23
8192	1.7440e-02	8.0233e-01	2.6949e-07	1.25
ooc	1.0	0.01	0.58	
eoc	2	1	1.5	1.5

Example 2 (unit cube)				
# elements	$\ \rho_N\ _\infty$	$\ \rho_N\ _2$	e_D , tol= 10^{-10}	ooc e_D
84	8.5418e-02	2.8696e-01	3.1694e01	
336	5.2286e-02	3.0612e-01	3.8364e00	3.05
1344	2.6438e-02	3.1681e-01	3.4635e00	0.15
5376	1.3784e-02	3.2257e-01	1.9136e00	0.86
ooc	0.89	-0.06	1.22	
eoc	2	1	1.5	1.5

Table 13: Convergence results with **Bempp** for Laplace BVP and introducing **Error B** (scaling diagonal of \mathbf{W}_h with factor $\frac{1}{2}$).

Example 1a (unit sphere)				
# elements	$\ \rho_N\ _\infty$	$\ \rho_N\ _2$	e_D , tol= 10^{-10}	ooc e_D
128	2.6579e02	1.6463e03	9.6177e-09	
512	1.3648e02	1.6128e03	3.7631e-08	-2.10*
2048	6.9163e01	1.6049e03	3.6792e-08	0.03*
8192	3.4849e01	1.6031e03	2.1073e-08	0.81*
ooc	1.00	0.01	-0.34*	
eoc	2	1	1.5	1.5

Example 2 (unit cube)				
# elements	$\ \rho_N\ _\infty$	$\ \rho_N\ _2$	e_D , tol= 10^{-10}	ooc e_D
84	1.7183e02	5.7502e02	1.1518e00	
336	1.0475e02	6.1184e02	1.1538e00	-0.003
1344	5.2853e01	6.3300e02	1.1540e00	-0.0003
5376	2.7539e01	6.4449e02	1.1540e00	0
ooc	0.89	-0.05	0.00	
eoc	2	1	1.5	1.5

Table 14: Convergence results with **Bempp** for Laplace BVP and introducing **Error C** (scaling diagonal of \mathbf{W}_h with factor 10^3).

*: Note that the values of e_D for Example 1a are in range of machine precision, hence the observed rate may be meaningless.

Example 1a (unit sphere)				
# elements	$\ \rho_N\ _\infty$	$\ \rho_N\ _2$	e_D , tol= 10^{-10}	ooc e_D
128	2.6579e02	1.1272e03	1.0095e00	
512	1.3648e02	1.1320e03	9.986e-01	0.02
2048	6.9163e01	1.1207e03	8.966e-01	0.16
8192	3.4895e01	1.1161e03	6.266e-01	0.52
ooc	1.00	0.01	0.23	
eoc	2	1	1.5	1.5

Example 2 (unit cube)				
# elements	$\ \rho_N\ _\infty$	$\ \rho_N\ _2$	e_D , tol= 10^{-10}	ooc e_D
84	1.5644e02	4.0097e03	9.4962e-01	
336	9.2386e01	4.1266e03	9.5179e-01	-0.03
1344	5.2853e01	4.5000e03	9.9276e-01	-0.06
5376	2.7539e01	4.7043e03	1.0096e00	-0.02
ooc	0.83	-0.08	-0.03	
eoc	2	1	1.5	1.5

Table 15: Convergence results with **Bempp** for Laplace BVP and introducing **Error D** (scaling first half of diagonal of \mathbf{W}_h with factor 10^3).

Example 1a (unit sphere)				
# elements	$\ \rho_N\ _\infty$	$\ \rho_N\ _2$	e_D , tol= 10^{-10}	ooc e_D
128	3.3031e-01	2.0450e00	2.4194e-08	
512	5.4697e-01	6.4588e00	9.5160e-09	1.44*
2048	6.6674e-01	1.5471e01	3.0787e-08	-1.72*
8192	7.3019e-01	3.3589e01	2.6546e-08	0.21*
ooc	-0.38	-1.4	-0.22*	
eoc	2	1	1.5	1.5

Example 2 (unit cube)				
# elements	$\ \rho_N\ _\infty$	$\ \rho_N\ _2$	e_D , tol= 10^{-10}	ooc e_D
84	2.3949e-01	8.0032e-01	8.080e-01	
336	3.9627e-01	2.3139e00	1.0560e00	-0.39
1344	4.5266e-01	5.4212e00	1.1301e00	-0.10
5376	4.9928e-01	1.1684e01	1.1483e00	-0.02
ooc	-0.34	-1.28	-0.16	
eoc	2	1	1.5	1.5

Table 16: Convergence results with **Bempp** for Laplace BVP and introducing **Error E** (scaling diagonal of \mathbf{W}_h with factor h^{-1}).

*: Note that the values of e_D for Example 1a are in range of machine precision, hence the observed rate may be meaningless.

4 Second Application: Time-Harmonic Maxwell's Equations

Let $k > 0$, we solve

$$\mathbf{curl} \mathbf{curl} u - k^2 u = 0 \quad \text{in } \mathbb{R}^3 \setminus \bar{\Omega},$$

with Silver-Müller radiation conditions. We will again start by considering what are the related functional spaces, for which we use the notation and definitions from [4, Sect. 2]. We will, however, be specific in the definition of the traces and BIOs, as there are different conventions in the literature and this will slightly change the concrete formula for the residuals, but obviously, the idea remains the same.

The weak solution of this exterior BVP $u \in \mathbf{H}_{loc}(\mathbf{curl}, \Omega)$, and we consider the tangential trace (sometimes referred as *twisted* tangential trace) $\gamma_{\times} : \mathbf{H}(\mathbf{curl}, \Omega) \rightarrow \mathbf{H}_{\times}^{-1/2}(\text{div}_{\Gamma}, \Gamma)$ and the magnetic trace $\gamma_R : \mathbf{H}_{loc}(\mathbf{curl}^2, \mathbb{R}^3 \setminus \Gamma) \rightarrow \mathbf{H}_{\times}^{-1/2}(\text{div}_{\Gamma}, \Gamma)$ defined as

$$\gamma_{\times} u := u|_{\Gamma} \times \mathbf{n}, \quad \text{and} \quad \gamma_R u := \gamma_{\times}(\mathbf{curl} u),$$

respectively, where the spaces are as defined in [4, Section 2]. Moreover, the related BIOs are

$$\mathsf{E}_k := \{\gamma_{\times}\}_{\Gamma} \circ \Psi_{SL,k}, \quad \mathsf{H}_k := \{\gamma_{\times}\}_{\Gamma} \circ \Psi_{DL,k},$$

where $\Psi_{SL,k}$ and $\Psi_{DL,k}$ are the single and double layer potentials as introduced in [4, Sect. 2 and 4, Eq.(27)-(28)]. We remark that E_k and H_k are continuous mappings from $\mathbf{H}_{\times}^{-1/2}(\text{div}_{\Gamma}, \Gamma)$ to $\mathbf{H}_{\times}^{-1/2}(\text{div}_{\Gamma}, \Gamma)$ when considering the *anti-symmetric* duality pairing

$$\langle \mathbf{u}, \mathbf{v} \rangle_{\times, \Gamma} := \int_{\Gamma} (\mathbf{u} \times \mathbf{n}) \cdot \mathbf{v} dS, \quad \mathbf{u}, \mathbf{v} \in \mathbf{L}_t^2(\Gamma), \quad (4.1)$$

but they map from $\mathbf{H}_{\times}^{-1/2}(\text{div}_{\Gamma}, \Gamma)$ to $\mathbf{H}_{\times}^{-1/2}(\mathbf{curl}_{\Gamma}, \Gamma)$ when considering the *symmetric* duality pairing

$$\langle \mathbf{u}, \mathbf{v} \rangle_{\Gamma} := \int_{\Gamma} \mathbf{u} \cdot \mathbf{v} dS, \quad \mathbf{u}, \mathbf{v} \in \mathbf{L}_t^2(\Gamma). \quad (4.2)$$

In the following, we will consider the symmetric duality pairing because that is what agrees with the implementations in `Bempp`. In order to test codes following other conventions, one just has to rotate the functions when needed, as will be done in the derivations later. However, as a consequence of the following Lemma, the rotations do not affect the computed convergence rates.

Lemma 4.1. *For $v \in \mathbf{H}_{\times}^{-1/2}(\mathbf{curl}_{\Gamma}, \Gamma)$ and \mathbf{n} the outward pointing normal vector, we have that*

$$\|v\|_{\mathbf{H}_{\times}^{-1/2}(\mathbf{curl}_{\Gamma}, \Gamma)} = \|\mathbf{n} \times v\|_{\mathbf{H}_{\times}^{-1/2}(\text{div}_{\Gamma}, \Gamma)}. \quad (4.3)$$

The proof can be found in Appendix A.

Now, let us return to the problem at hand. The corresponding Calderón identity for the exterior BVP is given by (see [4, Equation (34)])

$$\begin{pmatrix} \frac{1}{2} \mathsf{Id} - \mathsf{H}_k & -\mathsf{E}_k \\ -\mathsf{E}_k & \frac{1}{2} \mathsf{Id} - \mathsf{H}_k \end{pmatrix} \begin{pmatrix} \gamma_{\times} u \\ \gamma_R u \end{pmatrix} \iff \begin{pmatrix} \frac{1}{2} \mathsf{Id} + \mathsf{H}_k & \mathsf{E}_k \\ \mathsf{E}_k & \frac{1}{2} \mathsf{Id} + \mathsf{H}_k \end{pmatrix} \begin{pmatrix} \gamma_{\times} u \\ \gamma_R u \end{pmatrix} = 0. \quad (4.4)$$

Next, we proceed to discretize. We illustrate the procedure using Raviart-Thomas basis functions, and will comment on the difference when using Rao-Wilson-Glisson (RWG) basis functions afterwards.

Let \mathcal{G}_h be a given mesh of Γ . For $\mathbf{H}_\times^{-1/2}(\text{div}_\Gamma, \Gamma)$ we take the div-conforming lowest order Raviart-Thomas edge elements $\mathcal{RT}^0(\mathcal{G}_h)$ as defined in [7], while for $\mathbf{H}_\times^{-1/2}(\text{curl}_\Gamma, \Gamma)$ we consider the curl-conforming lowest order Nédélec edge elements $\mathcal{N}^0(\mathcal{G}_h)$ as introduced in [5, Sect. 7.2].

Let $\mathcal{P}_h : \mathbf{H}_\times^{-1/2}(\text{div}_\Gamma, \Gamma) \rightarrow \mathcal{RT}^0(\mathcal{G}_h)$ is the orthogonal projection from [4, Theorem 14]. Then, we have the following Calderón residuals

$$\begin{aligned} r_{M,1}(\psi) &= \int_\Gamma [\mathbf{E}_k \mathcal{P}_h(\gamma_R u) + (\frac{1}{2} \mathbf{Id} + \mathbf{H}_k) \mathcal{P}_h(\gamma_\times u)] \psi \, ds(x) \\ &= \int_\Gamma [\mathbf{E}_k (\mathcal{P}_h - \mathbf{Id})(\gamma_R u) + (\frac{1}{2} \mathbf{Id} + \mathbf{H}_k) (\mathcal{P}_h - \mathbf{Id})(\gamma_\times u)] \psi \, ds(x), \end{aligned} \quad (4.5)$$

$$\begin{aligned} r_{M,2}(\psi) &= \int_\Gamma [\mathbf{E}_k \mathcal{P}_h(\gamma_\times u) + (\frac{1}{2} \mathbf{Id} + \mathbf{H}_k) \mathcal{P}_h(\gamma_R u)] \psi \, ds(x) \\ &= \int_\Gamma [\mathbf{E}_k (\mathcal{P}_h - \mathbf{Id})(\gamma_\times u) + (\frac{1}{2} \mathbf{Id} + \mathbf{H}_k) (\mathcal{P}_h - \mathbf{Id})(\gamma_R u)] \psi \, ds(x) \end{aligned} \quad (4.6)$$

for $\psi \in \mathbf{H}_\times^{-1/2}(\text{curl}_\Gamma, \Gamma)$.

Now we can state the desired convergence result.

Theorem 4.2. *Let Ω_h be a tetrahedral mesh of Ω and let \mathcal{G}_h be a triangular surface mesh of Γ such that $\mathcal{G}_h = \Omega_h|_\Gamma$ up to geometric approximation of the boundary. Let $\beta_e, e = 1, \dots, N$ be a basis of $\mathcal{N}^0(\mathcal{G}_h)$. Let $r_{M,1}$ and $r_{M,2}$ be as introduced in (4.5) and (4.6), and define*

$$\boldsymbol{\rho}_{M,1} := [r_{M,1}(\beta_e)]_{e=1}^N, \quad \boldsymbol{\rho}_{M,2} := [r_{M,2}(\beta_e)]_{e=1}^N.$$

If the solution u of our exterior BVP is such that $\gamma_R u, \gamma_\times u \in \mathbf{H}_\times^1(\text{div}_\Gamma, \Gamma)$, then we have

$$\boxed{\begin{aligned} \|\boldsymbol{\rho}_{M,1}\|_\infty &= \mathcal{O}(h^1), & \|\boldsymbol{\rho}_{M,2}\|_\infty &= \mathcal{O}(h^1), \\ \|\boldsymbol{\rho}_{M,1}\|_2 &= \mathcal{O}(1), & \|\boldsymbol{\rho}_{M,2}\|_2 &= \mathcal{O}(1). \end{aligned}}$$

Proof. We only show the result for $\boldsymbol{\rho}_{M,1}$, as $\boldsymbol{\rho}_{M,2}$ can be obtained analogously. From (4.5), it follows that we have

$$\begin{aligned} |r_{M,1}| &\leq (\|\mathbf{E}_k\|_{\mathbf{H}_\times^{-1/2}(\text{div}_\Gamma, \Gamma) \rightarrow \mathbf{H}_\times^{-1/2}(\text{div}_\Gamma, \Gamma)} \|(\mathcal{P}_h - \mathbf{Id})\gamma_R u\|_{\mathbf{H}_\times^{-1/2}(\text{div}_\Gamma, \Gamma)} \\ &\quad + \|\frac{1}{2} \mathbf{Id} + \mathbf{H}_k\|_{\mathbf{H}_\times^{-1/2}(\text{div}_\Gamma, \Gamma) \rightarrow \mathbf{H}_\times^{-1/2}(\text{div}_\Gamma, \Gamma)} \|(\mathcal{P}_h - \mathbf{Id})\gamma_\times u\|_{\mathbf{H}_\times^{-1/2}(\text{div}_\Gamma, \Gamma)}) \|\psi\|_{\mathbf{H}_\times^{-1/2}(\text{curl}_\Gamma, \Gamma)} \end{aligned}$$

By continuity and [4, Thm 14] we get

$$|r_{M,1}| \leq c_1 h^{\frac{3}{2}} \|\psi\|_{\mathbf{H}_\times^{-1/2}(\text{curl}_\Gamma, \Gamma)} \quad (4.7)$$

for some constant $c_1 > 0$. We are interested in the decay rate when we take $\psi = \beta_e$, where β_e is a Nédélec basis function. We have that $\tilde{\beta}_e = \mathbf{n} \times \beta_e$, where $\tilde{\beta}_e$ is a Raviart-Thomas basis function. For a domain basis function b_e in $\mathcal{ND}_1(\Omega_h)$ (as defined in [6], with $\tilde{\beta}_e = \gamma_\times(b_e)$), it holds that $\|\tilde{\beta}_e\|_{\mathbf{H}_\times^{-1/2}(\text{div}_\Gamma, \Gamma)} \sim \|b_e\|_{H(\text{curl}, \Omega)}$, since

$$\|\gamma_\times b_e\|_{\mathbf{H}_\times^{-1/2}(\text{div}_\Gamma, \Gamma)} = \|\tilde{\beta}_e\|_{\mathbf{H}_\times^{-1/2}(\text{div}_\Gamma, \Gamma)} \leq \|b_e\|_{H(\text{curl}, \Omega)},$$

where we used the continuity of γ_{\times} in the last inequality. The other direction follows from [6, Lemma 5.7]. This equivalence is useful, since from Lemma 4.1 it holds that $\|\beta_e\|_{\mathbf{H}_{\times}^{-1/2}(\mathbf{curl}_{\Gamma}, \Gamma)} \sim \|\tilde{\beta}_e\|_{\mathbf{H}_{\times}^{-1/2}(\mathbf{div}_{\Gamma}, \Gamma)}$ and from [6] we know that $\|b_e\|_{H(\mathbf{curl}, \Omega)} \leq c_2 h^{-1/2}$ for some constant c_2 . Combining this with (4.7) gives the result. \square

Remark. Instead of using Raviart-Thomas and Nédélec basis functions in Theorem 4.2, we could also have chosen RWG and scaled Nédélec (SNC) basis functions. Let us denote, for simplicity, the basis functions of the Raviart-Thomas, RWG, Nédélec and scaled Nédélec function spaces by RT_i , RWG_i , NC_i and SNC_i . We remind the reader that the following relation holds between [9, Equation (17) and (18)]

$$\begin{aligned} RWG_i(r) &:= l_i RT_i(r), \\ SNC_i(r) &:= l_i NC_i(r), \end{aligned}$$

where l_i is the length of the edge where the basis function is defined.

This scaling factor means that when using RWG and SNC basis functions, we expect the convergence of the residuals to be of one order higher than what we obtained in Theorem 4.2.

4.1 Implementation and sanity checks

We use the following solutions to our exterior Maxwell BVP when Ω is the unit cube in \mathbb{R}^3 :

- **Example 3:** We consider the exact solution $U = \vec{p}e^{ik\vec{x}\cdot\vec{d}}$ with $\vec{p} = (1, 0, 0)^T$, $\vec{d} = (0, 0, 1)^T$ and $k = 1$.
- **Example 4:** We consider $U = (\vec{d} \times (\vec{p} \times \vec{d}))e^{ik\vec{x}\cdot\vec{d}}$ with $\vec{p} = (1.01, 0, 1.05)^T$, $\vec{d} = (0.57735, 0.57735, 0.57735)^T$ normalized, and $k = 2$.

4.1.1 Empiric convergence of norms of basis functions

We validate the predicted convergences rate of vectorial basis functions. In particular, we compute the $\mathbf{H}_{\times}^{-1/2}(\mathbf{div}_{\Gamma}, \Gamma)$ -norm for RWG basis functions $\tilde{\beta}_e$. We do this by inspecting the diagonals of the Galerkin matrices of the electric field integral operator \mathbf{E}_k with wavenumber $k = i$. Note that calculating this gives a measure of the square of the norms of the basis functions, and thus we compare them with two times the computed convergence estimate. In Table 17 we see that the observed convergence rates for all of the basis functions are close to the expected ones.

# elements	$\max(\text{diag}(\mathbf{E}_{i,h}))$
24	4.153e-01
96	2.373e-01
384	1.174e-01
1536	5.851e-02
6144	2.923e-02
observed conv. rate	0.968
expected conv. rate	1

Table 17: Maximal element on diagonal of \mathbf{E}_h with wavenumber $k = i$ to estimate convergence of RWG basis functions

4.1.2 Checking convergence of Calderón residuals

In this section we verify our estimates for Calderón residuals. We remark that **Bempp** uses SNC and RWG functions, which we will denote by $\mathcal{E}^0(\mathcal{G}_h) \subset \mathbf{H}_x^{-1/2}(\mathbf{curl}_\Gamma, \Gamma)$ and $\mathcal{E}_x^0(\mathcal{G}_h) \subset \mathbf{H}_x^{-1/2}(\mathbf{div}_\Gamma, \Gamma)$, respectively. The **Bempp** results can be found in Table 18. From Remark 4, we predict to have $\|\rho_{M,i}\|_\infty = \mathcal{O}(h^2)$ and $\|\rho_{M,i}\|_2 = \mathcal{O}(h)$ for $i = 1, 2$. We see that for both Examples we obtain a convergence rate of approximately one order higher than we expected.

Example 4				
# elements	$\ \rho_{M,1}\ _2$	$\ \rho_{M,1}\ _\infty$	$\ \rho_{M,2}\ _2$	$\ \rho_{M,2}\ _\infty$
24	2.16776e-01	5.76130e-02	3.62201e-01	8.23841e-02
96	4.64068e-02	8.96662e-03	6.41830e-02	1.15569e-02
384	1.01251e-02	1.11766e-03	1.19495e-02	1.31189e-03
1536	2.37529e-03	1.48827e-04	2.54622e-03	1.62684e-04
6144	5.74156e-04	1.91928e-05	5.90082e-04	2.00978e-05
observed conv. rate	2.14	2.90	2.32	3.02
expected conv. rate	1	2	1	2

Example 5				
# elements	$\ \rho_{M,1}\ _2$	$\ \rho_{M,1}\ _\infty$	$\ \rho_{M,2}\ _2$	$\ \rho_{M,2}\ _\infty$
24	1.88446e-01	7.66625e-02	2.86437e-01	8.04880e-02
96	3.22867e-02	5.74773e-03	4.73946e-02	9.75907e-03
384	5.69888e-03	4.92157e-04	7.76580e-03	8.36725e-04
1536	1.19773e-03	7.17868e-05	1.43842e-03	7.48340e-05
6144	2.82986e-04	9.43459e-06	3.08229e-04	8.56077e-06
observed conv. rate	2.35	3.23	2.48	3.22
expected conv. rate	1	2	1	2

Table 18: Calderón residuals for Maxwell BVP.

4.2 Numerical results when introducing artificial errors

As before, for each test, we calculate the Calderón residuals, compare them with the standard *MMS* convergence test. In other words, we do the following convergence test: (i) We build the *correct* Galerkin matrices and store them as \mathbf{E}_h and \mathbf{H}_h . We also build the mass matrix \mathbf{M}_h arising from *Id*; (ii) we introduce an artificial error in the computation of the matrix of \mathbf{E} , and store the *defective* Galerkin matrix as \mathbf{E}_h^e ; (iii) We use GMRES with relative tolerance 10^{-10} . to numerically solve the following linear systems

$$\mathbf{E}_h^e \vec{w} = \left(\frac{1}{2} \mathbf{M}_h - \mathbf{H}_h \right) \tilde{\mathcal{P}}_h \gamma \times u \quad (4.8)$$

for the coefficient vectors \vec{w} ; (iv) We measure the *MMS* error

$$\mathbf{e}_R := \|\gamma_R u - w_h\|_{\mathbf{H}_x^{-1/2}(\mathbf{div}_\Gamma, \Gamma)} \approx ((\mathcal{P}_h \gamma_R u - \vec{w})^\top \mathbf{E}_h (\mathcal{P}_h \gamma_R u - \vec{w}))^{\frac{1}{2}}; \quad (4.9)$$

(v) Finally, we repeat steps (i)-(iv) for a sequence of dyadically refined meshes and see if this behaves like $\mathcal{O}(h^{\frac{3}{2}})$, where h is the meshwidth as before. Note that in all tables where we measure \mathbf{e}_R , the columns labelled ‘ooc \mathbf{e}_R ’, contain the observed convergence rate calculated using the error of two consecutive meshsizes.

4.2.1 Inaccurate quadrature

We adapt the quadrature for Example 3. Standard parameters in Bempp are order 4 for both the singular and the regular quadrature. These are adapted to 1 for the singular and 2 for the regular quadrature, respectively. In Table 19, we see that adapting the quadrature does not do enough damage to destroy the convergence of the Calderón residuals, and also the convergence result from the MMS test, i.e., from calculating (4.9), gives us a higher rate than expected.

# elements	$\ \rho_{M,1}\ _2$	$\ \rho_{M,1}\ _\infty$	$\ \rho_{M,2}\ _2$	$\ \rho_{M,2}\ _\infty$	e_R , tol=10 ⁻¹⁰	ooc e_R
24	2.079e-01	6.594e-02	3.301e-01	7.537e-02	1.211e00	
96	3.709e-02	7.372e-03	5.446e-02	9.329e-03	4.006e-01	1.60
384	8.142e-03	8.703e-04	1.004e-02	1.045e-03	1.117e-01	1.84
1536	1.897e-03	1.081e-04	2.082e-03	1.214e-04	2.952e-02	1.92
6144	4.574e-04	1.400e-05	4.747e-04	1.490e-05	7.786e-03	1.92
ooc	2.19	3.05	2.36	3.09	1.83	
eoc	1	2	1	2	1.5	1.5

Table 19: Calderón residuals with Bempp for Maxwell BVP, considering Example 3 and using less quadrature points.

4.2.2 Adapting entries in \mathbf{E}_h

In order to be consistent with the previous numerical experiments, we investigate what happens when we introduce the following artificial errors:

- [Error A] replacing the diagonal of \mathbf{E}_h with random numbers between 0 and 10,
- [Error B] scaling the diagonal of \mathbf{E}_h with a factor $\frac{1}{2}$,
- [Error C] scaling the diagonal of \mathbf{E}_h with a factor 10^3 ,
- [Error D] scaling the first half of the diagonal of \mathbf{E}_h with a factor 10^3 ,
- [Error E] scaling the diagonal of \mathbf{E}_h with a factor h^{-1} , where h is the meshwidth.

# elements	$\ \rho_{M,1}\ _2$	$\ \rho_{M,1}\ _\infty$	$\ \rho_{M,2}\ _2$	$\ \rho_{M,2}\ _\infty$	e_R , tol=10 ⁻¹⁰	ooc e_R
24	6.713e-01	2.218e-01	6.543e-01	2.527e-01	4.998e-01	
96	6.565e-01	1.612e-01	6.215e-01	1.733e-01	1.525e-01	1.71
384	7.217e-01	8.728e-02	7.257e-01	8.791e-02	4.158e-02	1.87
1536	7.248e-01	4.410e-02	7.063e-01	4.421e-02	1.209e-02	1.78
6144	7.117e-01	2.209e-02	7.064e-01	2.209e-02	3.618e-03	1.74
ooc	-0.03	0.85	-0.04	0.90	1.8	
eoc	1	2	1	2	1.5	1.5

Table 20: Convergence results with Bempp for one instance of the Maxwell BVP using Example 3 and introducing Error A (replacing diagonal entries of \mathbf{V}_h with random numbers).

Error A: Table 20 shows the results when replacing the diagonal of the Galerkin matrix \mathbf{E}_h of \mathbf{E}_h with random numbers. We see that while the observed convergence rate

for the Calderón residuals is less than we expected, the rate from the MMS test in (4.9) is higher than expected. We therefore see that the Calderón residual test is able to detect the introduced error, while the standard MMSs test is not.

Error B-D: Tables 21-23 report the results when we multiply the diagonal of \mathbf{E}_h by different h -independent constants. There, the observed convergence rates are everywhere larger than the expected rates, which means that both tests agree on their results.

# elements	$\ \rho_{M,1}\ _2$	$\ \rho_{M,1}\ _\infty$	$\ \rho_{M,2}\ _2$	$\ \rho_{M,2}\ _\infty$	e_R , tol=10 ⁻¹⁰	ooc e_R
24	1.185e-01	3.399e-02	2.717e-01	5.778e-02	7.151e-01	
96	2.805e-02	4.590e-03	3.777e-02	6.276e-03	1.120e-01	2.67
384	8.793e-03	8.437e-04	8.174e-03	8.027e-04	3.546e-02	1.66
1536	2.608e-03	1.205e-04	2.4311e-03	1.176e-04	1.236e-02	1.52
6144	7.159e-04	1.558e-05	6.889e-04	1.539e-05	4.909e-03	1.33
ooc	1.81	2.74	2.12	2.95	1.8	
eoc	1	2	1	2	1.5	1.5

Table 21: Convergence results with `Bempp` for Maxwell BVP using Example 3 and introducing Error B (diving values on diagonal of \mathbf{E}_h by two).

# elements	$\ \rho_{M,1}\ _2$	$\ \rho_{M,1}\ _\infty$	$\ \rho_{M,2}\ _2$	$\ \rho_{M,2}\ _\infty$	e_R , tol=10 ⁻¹⁰	ooc e_R
24	2.783e02	6.276e01	2.784e02	6.278e01	4.8284e-01	
96	9.028e01	1.916e01	9.030e01	1.916e01	1.4313e-017	1.75
384	2.469e01	2.424e00	2.469e01	2.424e00	4.1327e-02	1.79
1536	6.401e00	3.040e-01	6.401e00	3.040e-01	1.2059e-02	1.78
6144	1.626e00	3.803e-02	1.626e00	3.803e-02	3.6064e-03	1.74
ooc	1.87	2.74	1.87	2.74	1.8	
eoc	1	2	1	2	1.5	1.5

Table 22: Convergence results with `Bempp` for Maxwell BVP using Example 3 and introducing Error C (scaling diagonal of \mathbf{E}_h by 10³).

# elements	$\ \rho_{M,1}\ _2$	$\ \rho_{M,1}\ _\infty$	$\ \rho_{M,2}\ _2$	$\ \rho_{M,2}\ _\infty$	e_R , tol=10 ⁻¹⁰	ooc e_R
24	1.911e02	6.276e01	2.012e02	6.278e01	8.5126e-01	
96	6.126e01	1.916e01	6.338e01	1.916e01	1.3188e-01	2.69
384	1.692e01	2.424e00	1.732e01	2.424e00	4.6648e-02	1.78
1536	4.465e00	3.040e-01	4.498e00	3.040e-01	1.4739e-02	3.16
6144	1.142e00	3.803e-02	1.147e00	3.803e-02	4.2723e-03	1.79
ooc	1.86	2.74	1.87	2.74	1.8	
eoc	1	2	1	2	1.5	1.5

Table 23: Convergence results with `Bempp` for Maxwell BVP using Example 3 and introducing Error D (scaling first half of diagonal of \mathbf{E}_h by 10³).

Error E: Table 24 displays the results when scaling the diagonal of \mathbf{E}_h by a factor h^{-1} , where h is the meshwidth (computed as average size of an element in **Bempp**). We see that while the observed convergence rates for Calderón residuals are lower than expected, the rate in $\mathbf{H}_x^{-1/2}(\text{div}_\Gamma, \Gamma)$ -norm still is higher than we expected. Therefore, the Calderón residual test detects the introduced error, while the standard test does not.

# elements	$\ \boldsymbol{\rho}_{M,1}\ _2$	$\ \boldsymbol{\rho}_{M,1}\ _\infty$	$\ \boldsymbol{\rho}_{M,2}\ _2$	$\ \boldsymbol{\rho}_{M,2}\ _\infty$	ϵ_R , tol=10 ⁻¹⁰	ooc ϵ_R
24	1.278e00	2.669e-01	1.381e00	2.916e-01	1.1026e00	
96	8.329e-01	1.770e-01	8.480e-01	1.799e-01	1.4364e-01	2.94
384	4.667e-01	4.620e-02	4.688e-01	4.641e-02	4.1157e-02	1.80
1536	2.461e-01	1.176e-02	2.463e-01	1.178e-02	1.2049e-02	1.77
6144	1.263e-01	2.963e-03	1.263e-01	2.964e-03	3.6062e-03	1.74
ooc	0.84	1.69	0.87	1.72	2.0	
eoc	1	2	1	2	1.5	1.5

Table 24: Convergence results with **Bempp** for Maxwell BVP using Example 3 and introducing Error E (scaling diagonal of \mathbf{E}_h by h^{-1}).

5 Summary and Discussion

In this summary, we use the following notation:

- ‘✗’ if the convergence rate is lower than expected, which means the test says ”example fails to be correct“;
- ‘✓’ if the convergence rate is higher or deviates less than 10% from what we predicted, which means the test says ”example is correct“;
- ‘*’ when the obtained errors for all refinement meshes are within machine precision, so we cannot use the convergence rate to make a conclusion, but it is clear that no errors were detected;
- ‘⊗’ when the convergence rates for the ‘MMS test’ fluctuate, from which we conclude that the test fails.

The idea is to compare the outputs of the Calderón residual test (dubbed ‘Calderón test’ for short), and the MMS tests from (3.9), (3.10), and (4.9) (labelled ‘MMS’ in the tables). In particular, we do not think it is a problem that the Calderón residual test is unable to detect errors in the matrix entries when the standard MMS test also fails to notice. Hence, we also consider in our summary whether the outputs agree or not. We remark that for the MMS test, our conclusion follows the convergence rates calculated between consecutive refinement levels and not the linear regression based on all results, since in some cases there are large differences between the computation methods.

It turns out that the Calderón residual estimates that we proposed in this paper did not provide the robust debugging tool that we had hoped for. Yet, from our numerical experiments, we believe that it can still be useful in some circumstances. Indeed, we see in Table 25 that in the case of \mathbf{W} for Example 2 of the Laplacian, the Calderón residual test is always able to detect errors. However, for that BVP, it is unreliable for \mathbf{V} . Even if it does work for some introduced errors, this is not helpful because we do not know a priori what the problem is when debugging.

Weakly singular operator V						
	Example 1a			Example 2		
Artificial Error	Calderón test	MMS	Agree?	Calderón test	Norm test	Agree?
Error A	\times	\circledast	yes	\times	\times	yes
Error B	\checkmark	\checkmark	yes	\times	\times	yes
Error C	\checkmark	*	yes	\checkmark	\times	no
Error D	\checkmark	*	yes	\checkmark	\times	no
Error E	\times	*	no	\times	\times	yes
Hypersingular operator W						
	Example 1a			Example 2		
Artificial Error	Calderón test	MMS	Agree?	Calderón test	Norm test	Agree?
Error A	\times	\circledast	yes	\times	\times	yes
Error B	\times	\times	yes	\times	\times	yes
Error C	\times	*	no	\times	\times	yes
Error D	\times	\times	yes	\times	\times	yes
Error E	\times	*	no	\times	\times	yes

Table 25: Summary of convergence results for Laplace BPV.

Electric Field Integral operator E_k			
Artificial Error	Calderón test	Norm test	Agree?
Error A	\times	\checkmark	no
Error B	\checkmark	\checkmark	yes
Error C	\checkmark	\checkmark	yes
Error D	\checkmark	\checkmark	yes
Error E	\times	\checkmark	no

Table 26: Summary of convergence results for Maxwell BPV.

In the case of the EFIE, the MMS test seems to always be oblivious to the introduced errors. That means that these do not affect the solution of the boundary integral equation, and hence, it is hard to decide whether it is relevant that the Calderón residual test does ring the alarm in some cases.

In spite of our disappointment, we believe it is worth reporting these findings. On the one hand, it may be useful for some practitioners, and then it is important that they are aware of the shortcomings of this technique. On the other hand, it may be possible in the future to make these estimates sharper.

Acknowledgments

The authors based in Delft would like to thank Kees Vuik for his valuable feedback in an earlier version of the numerical results Section. A.W. would like to acknowledge D. Hoonhout and J. Wallaart for their IT support. This work has been partially funded by the Dutch Research Council (NWO) under the NWO-Talent Programme Veni with the project number VI.Veni.212.253.

References

- [1] A Buffa and P Ciarlet Jr. On traces for functional spaces related to Maxwell's equations. I. An integration by parts formula in Lipschitz polyhedra. *Math. Methods Appl. Sci.*, 24:9–30, 2001.
- [2] A Buffa and P Ciarlet Jr. On traces for functional spaces related to Maxwell's equations. II. Hodge decompositions on the boundary of Lipschitz polyhedra and applications. *Math. Methods Appl. Sci.*, 24:31–48, 2001.
- [3] A. Buffa, M. Costabel, and D. Sheen. On traces for $\mathbf{H}(\mathbf{curl}, \Omega)$ in Lipschitz domains. *J. Math. Anal. Appl.*, 276:845–867, 2002.
- [4] A Buffa and R Hiptmair. Galerkin boundary element methods for electromagnetic scattering. *Topics in Computational Wave Propagation, Lect. Notes Comput. Sci. Eng*, 31:85–126, 01 2003.
- [5] R. Hiptmair. Boundary element methods for eddy current computation. In *Boundary element analysis*, volume 29 of *Lect. Notes Appl. Comput. Mech.*, pages 213–248. Springer, Berlin, 2007.
- [6] R Hiptmair and S Mao. Stable multilevel splittings of boundary edge element spaces. *Bit. Numer. Math*, 52:661–685, 01 2012.
- [7] P.-A. Raviart and J. M. Thomas. A mixed finite element method for 2nd order elliptic problems. pages 292–315. Lecture Notes in Math., Vol. 606, 1977.
- [8] S.A. Sauter and C. Schwab. *”Boundary Element Methods”*. Springer, 2011.
- [9] Matthew W. Scroggs, Timo Betcke, Erik Burman, Wojciech Śmigaj, and Elwin van 't Wout. Software frameworks for integral equations in electromagnetic scattering based on calderón identities. *Computers & Mathematics with Applications*, 74(11):2897–2914, 2017.
- [10] O. Steinbach. *”Numerical Approximation Methods for Elliptic Boundary Value Problems”*. Springer, 2008.

A Proof of Lemma 4.1

Proof. Let us recall the following definitions and relations between spaces from [1, 2, 3, 4].

- $H_T^{1/2}(\Gamma) := \{\gamma_T(u) := n \times (u|_\Gamma \times n), u \in H^1(\Omega)^3\}$,
 $\|p\|_{H_T^{1/2}(\Gamma)} := \inf\{\|u\|_{H^1(\Omega)} | \gamma_T u = p\}$,
- $H_R^{1/2}(\Gamma) := \{v | n \times v \in H_T^{1/2}(\Gamma)\}$, $\|q\|_{H_R^{1/2}(\Gamma)} := \|n \times q\|_{H_T^{1/2}(\Gamma)}$,
- $H_T^{-1/2}(\Gamma) := H_R^{1/2}(\Gamma)', H_R^{-1/2}(\Gamma) := H_T^{1/2}(\Gamma)' \text{ (using the symmetric pairing)}$
- $\mathbf{H}_\times^{-1/2}(\text{div}_\Gamma, \Gamma) := \{\mu \in H_R^{-1/2}(\Gamma) | \text{div}_\Gamma \mu \in H^{-1/2}(\Gamma)\}$,
 $\|\mu\|_{\mathbf{H}_\times^{-1/2}(\text{div}_\Gamma, \Gamma)} := \|\mu\|_{H_R^{-1/2}(\Gamma)} + \|\text{div}_\Gamma \mu\|_{H^{-1/2}(\Gamma)}$
- $\mathbf{H}_\times^{-1/2}(\mathbf{curl}_\Gamma, \Gamma) := \{\mu \in H_T^{-1/2}(\Gamma) | \mathbf{curl}_\Gamma \mu \in H^{-1/2}(\Gamma)\}$,
 $\|\mu\|_{\mathbf{H}_\times^{-1/2}(\mathbf{curl}_\Gamma, \Gamma)} := \|\mu\|_{H_T^{-1/2}(\Gamma)} + \|\mathbf{curl}_\Gamma \mu\|_{H^{-1/2}(\Gamma)}$.

Since it holds that $\mathbf{curl}_\Gamma v = \operatorname{div}_\Gamma(\mathbf{n} \times v)$ for $v \in \mathbf{H}_\times^{-1/2}(\mathbf{curl}_\Gamma, \Gamma)$, we only need to show that

$$\|v\|_{H_T^{-1/2}(\Gamma)} = \|\mathbf{n} \times v\|_{H_R^{-1/2}(\Gamma)}. \quad (\text{A.1})$$

Let $\mathbf{R} u := \mathbf{n} \times u : H_R^{1/2}(\Gamma) \rightarrow H_T^{1/2}(\Gamma)$. From [3, Equation (16) and below] it then follows that $\mathbf{R}^{-1} = \mathbf{R}^* = -\mathbf{R}$. Hence

$$\begin{aligned} \|v\|_{H_T^{-1/2}(\Gamma)} &= \sup_{w \in H_R^{1/2} \setminus \{0\}} \frac{|\langle v, w \rangle_{H_T^{-1/2}(\Gamma) \times H_R^{1/2}(\Gamma)}|}{\|w\|_{H_R^{1/2}(\Gamma)}} \\ &= \sup_{\mathbf{R} w \in H_R^{1/2} \setminus \{0\}} \frac{|\langle \mathbf{R}^* \mathbf{R} v, w \rangle_{H_T^{-1/2}(\Gamma) \times H_R^{1/2}(\Gamma)}|}{\|\mathbf{R} w\|_{H_T^{1/2}(\Gamma)}} \\ &= \sup_{u \in H_R^{1/2} \setminus \{0\}} \frac{|\langle \mathbf{R} v, u \rangle_{H_R^{-1/2}(\Gamma) \times H_T^{1/2}(\Gamma)}|}{\|u\|_{H_T^{1/2}(\Gamma)}} = \|\mathbf{R} v\|_{H_R^{-1/2}(\Gamma)}. \end{aligned} \quad (\text{A.2})$$

□

B Additional observations

Consider the following setting: let Ω be the unit cube in 3D, and choose real numbers a_1, a_2 and a_3 such that $\sum_{i=1}^3 a_i = 0$. Then

$$u(x, y, z) = a_1 x^2 + a_2 y^2 + a_3 z^2$$

is a solution to the Laplace equation on Ω . Then

$$\tau_N u = \begin{pmatrix} 2a_1 x \\ 2a_2 y \\ 2a_3 z \end{pmatrix} \cdot \mathbf{n}|_\Gamma = \begin{cases} 0, & x = 0 \\ 2a_1, & x = 1 \\ 0, & y = 0 \\ 2a_2, & y = 1 \\ 0, & z = 0 \\ 2a_3, & z = 1, \end{cases}$$

which consists of piecewise constant functions. This means that $\mathcal{I}_h^{p-1, -1} \tau_N u = \tau_N u$ in this case. In Example 2 we are in this situation. Then, the residuals (3.2) and (3.3) become

$$\begin{aligned} r_D(\psi) &:= \int_\Gamma [(\frac{1}{2} \mathbf{Id} - \mathbf{K}) \mathcal{I}_h^{p, 0}(\tau_D u)](x) \psi(x) dS(x) + \mathbf{V}(\mathcal{I}_h^{p-1, -1} \tau_N u)(x) \psi(x) dS(x) \\ &= \int_\Gamma [(\frac{1}{2} \mathbf{Id} - \mathbf{K}) (\mathcal{I}_h^{p, 0} - \mathbf{Id})(\tau_D u)](x) \psi(x) dS(x), \end{aligned} \quad (\text{B.1})$$

and

$$\begin{aligned} r_N(\phi) &:= \int_\Gamma [\mathbf{W} \mathcal{I}_h^{p, 0}(\tau_D u)](x) \phi(x) dS(x) + (\frac{1}{2} \mathbf{Id} + \mathbf{K}') \mathcal{I}_h^{p-1, -1} \tau_N u](x) \phi(x) dS(x) \\ &= \int_\Gamma [\mathbf{W} (\mathcal{I}_h^{p, 0} - \mathbf{Id})(\tau_D u)](x) \phi(x) dS(x), \end{aligned} \quad (\text{B.2})$$

which are slightly simpler forms, and might help with identifying which terms contribute to the fact that we numerically observe higher convergence rates.

C Eigenvalues corresponding to matrices with artificial errors for \mathbf{V}_h

In this Appendix we take a closer look at what is happening when we introduce **Error B**, i.e., when we scale the diagonal of \mathbf{V}_h with a factor $1/2$. Figures 1 and 2 display the eigenvalues of the original matrix \mathbf{V}_h and the resulting scaled matrix \mathbf{V}_h^e for Examples 1a and 2, respectively. In both cases, we are considering the smallest mesh. We see in these plots that scaling the diagonal of \mathbf{V}_h with a factor $\frac{1}{2}$ shifts down the spectra. When this is done, quite a lot of the eigenvalues of \mathbf{V}_h^e are now negative, and the matrix is thus no longer symmetric positive definite. This may be one of the reasons why the iterative solvers we tried, namely CG and GMRES, failed.

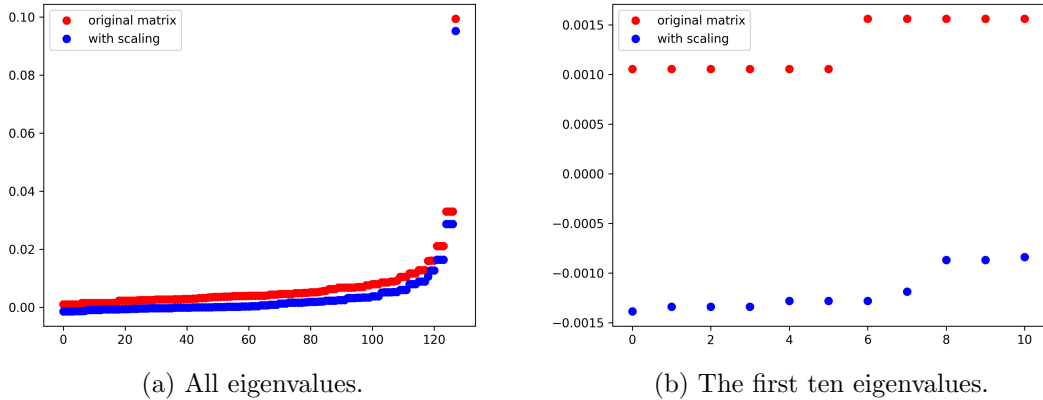


Figure 1: Eigenvalues when scaling the diagonal of \mathbf{V}_h by $1/2$ in Example 1a for the Laplacian (**Error B**). Results for smallest mesh, i.e., $N = 128$ elements.

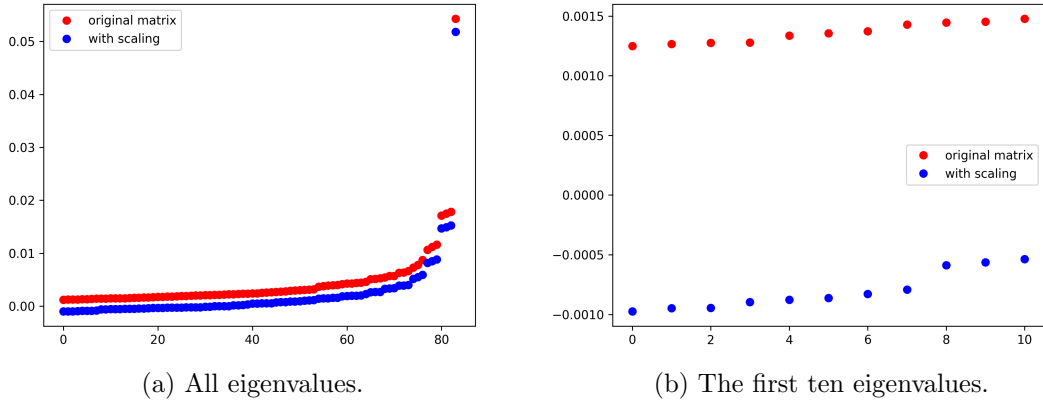


Figure 2: Eigenvalues when scaling the diagonal of \mathbf{V}_h by $1/2$ in Example 2 for the Laplacian (**Error B**). Results for smallest mesh, i.e., $N = 84$ elements.